ISSN: 2277-9655
Impact Factor: 4.116

IJESRT

INTERNATIONAL JOURNAL OF ENGINEERING SCIENCES & RESEARCH TECHNOLOGY

THEORETICAL COMPARATIVE STUDY OF INTERNAL QUANTUM EFFICIENCY OF THIN FILMS SOLAR CELLS BASED ON $CuInSe_2$: $p^+/p/n/n^+$, $p/n/n^+$, $p^+/p/n$ and p/n MODELS

E.M. Keita *, B. Mbow, M.L. Sow , C. Sow , M. Thiam , C. Sene
Laboratoire des Semiconducteurs et d'Energie solaire, Département de Physique, Faculté des Sciences et Techniques, Université Cheikh Anta Diop, Dakar, Sénégal

DOI: 10.5281/zenodo.154202

ABSTRACT

In this paper we propose to study the performances of thin films solar cells based on $CuInSe_2$. The following models are studied : p/n ; $p^+/p/n$; $p/n/n^+$; $p^+/p/n/n^+$. The objective of this work is to study the performance of the homojunction based on $CuInSe_2$, with a medium band gap window layer based on $CuInS_2$, deposited on a substrate, according to the model $CuInS_2(p^+)/CuInSe_2(p)/CuInSe_2(n)/CuInSe_2(n^+)$ ($p^+/p/n/n^+$). We compare this structure ($p^+/p/n/n^+$) with the following models: the homojunction $CuInSe_2(p)/CuInSe_2(n)$ (p/n), the homojonction with window layer $CuInS_2(p^+)/CuInSe_2(p)/CuInSe_2(n)$ ($p/n/n^+$) and the homojunction deposited on substrate $CuInSe_2(p)/CuInSe_2(n)/CuInSe_2(n^+)$ ($p/n/n^+$). Calculation models for determining the density of the minority carriers, the density of the photocurrent, and the internal quantum efficiency were established for the different structures. These theoretical results are used to compare their performance. In order to test the validity of our calculations models, We compare our results with some experimental results published in the literature.

KEYWORDS: Thin films, $CuInSe_2$, $CuInS_2$, Two - three and four layers models, Internal quantum efficiency, short-circuit photocurrent.

INTRODUCTION

Homojunction based on $CuInSe_2(p)/CuInSe_2(n)$ is often characterized by the losses of carriers by recombination phenomenon at the front layer surface (illuminated face). To reduce the recombination velocity at the surface, a window layer having a lattice matched to the absorbent layer [1] is often deposited on the front surface. In the range of low energies corresponding to lower absorption cofficients, the photons reach the rear area (depth absorption), the effects of the base and the back surface become important. The deposition of a substrate on the back surface allows to reduce the losses of carriers on the back side and confine minority photocarriers in the base (creating a low potential barrier) in order to increase their collect at the junction.

In this work the models of cell used are the homojunction model $CuInSe_2(p)/CuInSe_2(n)$, the homojunction with window layer model $CuInS_2(p^+)/CuInSe_2(p)/CuInSe_2(n)$, the homojunction deposited on a substrate model $CuInSe_2(p)/CuInSe_2(n)/CuInSe2(n^+)$ and the homojunction with window layer deposited on a substrate model $CuInS_2(p^+)/CuInSe_2(p)/CuInSe_2(n)/CuInSe_2(n^+)$.

The $CuInSe_2$ has a direct band gap in order to 1.04 eV [2-5] and a lattice matched to the $CuInS_2$ (see Table 1). The band gap of the $CuInS_2$ is in the order of 1.57 eV [6], this material can be used as a window layer for photons energies ranging from 1.04 eV to 1.57 eV.

The substrate doped n^+ and the base doped n are the same family, the interface effects are neglected because there is a continuity of layers. The n^+ doping allows to maintain photocarriers in the base (creating a low potential barrier).

To represent the real structure of our solar cell, a theoretical study, based on solving a system of differential equations formed by the continuity equations, is developed. The solution of these equations depends on the boundary conditions used in the different regions of the structure. However, the literal solution of this problem allows to have precious information for the characterization and the optimization of geometrical and electrical parameters of the different layers. It also allows to choose the best structure in order to enhance the cell performance.

MATERIALS AND METHODS

For each structure, a theoretical model is proposed for determining the quantum internal efficiency and the short-circuit photocurrent. It is assumed that the optical reflection coefficient is neglected at each interface in the spectral range used. It is also considered that the space charge region is located only between the p and n regions of each structure and there is no electric field outside this region. We neglect recombination phenomena in the space charge region.

The Table 1 lists the different physical parameters used in this work for each structure [6 - 12].

Table 1. physical parameters used in this work [6 - 12]

Material	E_g (gap)	a	c	X (electron affinity)	Type (p,n)
$CuInSe_2$ (p,n)	0.96 – 1.04 eV	5.78 Å	11.62 Å	4.58 eV	10^{14}- 10^{20} cm^{-3}
$CuInS_2$ (p)	1.438 – 1.57 eV	5.51 Å	11 Å	4.04 eV	10^{16}- 10^{20} cm^{-3}

The absorption coefficients of the different materials ($CuInSe_2$ and $CuInS_2$) used in this work are shown on figure 1. We used the values of the absorption coefficients given by Subba Ramaiah Kodigala [6] for photon energies ranging from 1 to 2 eV. We have approximately completed these values for photon energies greater than 2 eV.

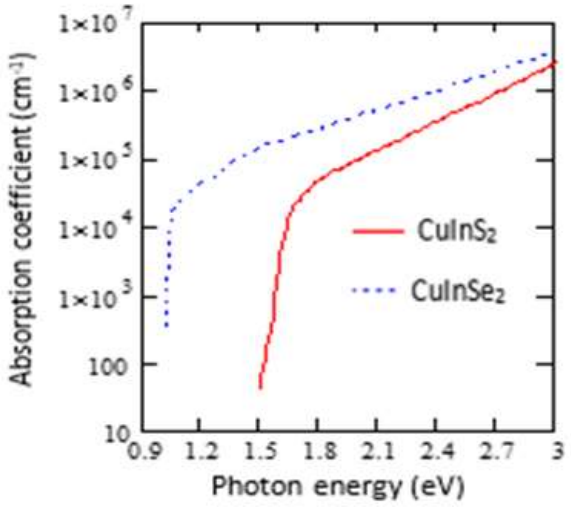

Figure 1. Absorption coefficient versus photon energy

First, we propose to study the structure $p^+/p/n/n^+$ (4 layers model). The results obtained with this model allow to deduce easily those which correspond to the other structures : p/n (2 layers model), $p^+/p/n$ et $p/n/n^+$ (3 layers model).

The energy band diagram is based on the Anderson model [13], it depends of the electronic properties as the electron affinity, the width of the band gap and the doping level (see Table 1).

We pose :

$\Delta E_{c0} = -(\chi_{\mathrm{CuInSe2}} - \chi_{\mathrm{CuInS2}})$, or : $\Delta E_{c0} = -0.54\ eV$

$\Delta E_g = E_{g\mathrm{CuInSe2}} - E_{g\mathrm{CuInS2}}$, or : $\Delta E_g = -0.53\ eV$

$\Delta E_{v0} = \Delta E_{c0} - \Delta E_g$, or : $\Delta E_{v0} = -0.01\ eV$

ISSN: 2277-9655
Impact Factor: 4.116

The diagrams of the structure and the energy band are respectively shown in Figures 2 and 3.

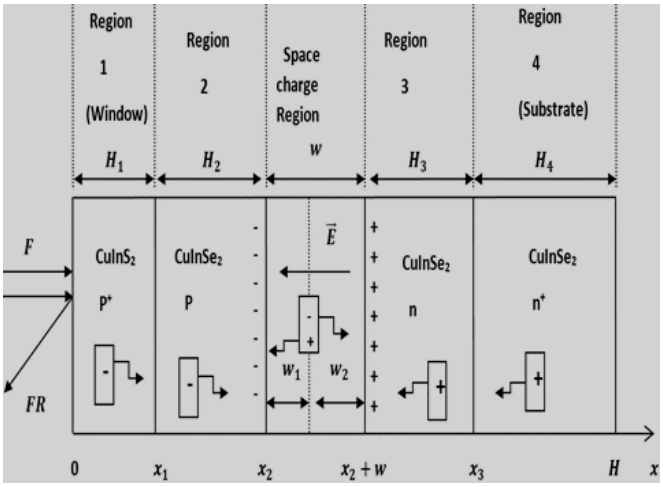

Figure 2. diagram of the structure $CuInS_2(p^+)/CuInSe_2(p)/CuInSe_2(n)/CuInSe_2(n^+)$

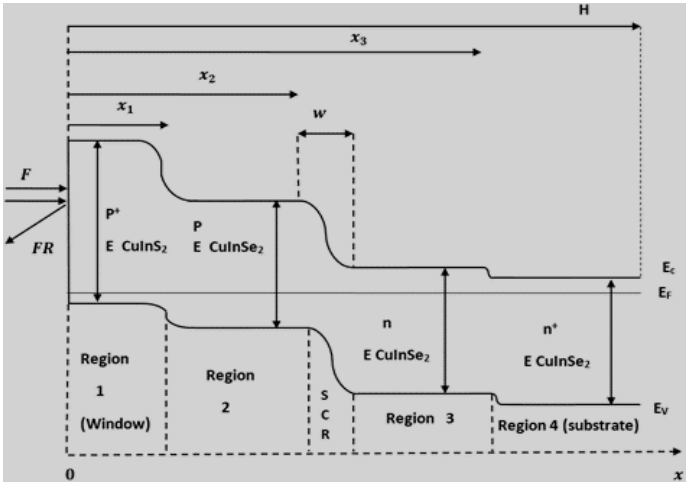

Figure 3. Energy band diagram of the structure $CuInS_2(p^+)/CuInSe_2(p)/CuInSe_2(n)/CuInSe_2(n^+)$

2-1. Calculation of the photocurrent in region 1 (window layer)

In region 1 (window layer), $0 \le x \le x_1$, the photocurrent is essentially due to the electrons, the continuity equation is:

$$\frac{d^2\Delta n_1}{dx^2} - \frac{\Delta n_1}{{L_{n_1}}^2} = \frac{-\alpha_1 F(1-R)e^{-\alpha_1 x}}{D_{n_1}} \quad (2\text{-}1)$$

With ${L_{n_1}}^2 = D_{n_1}\tau_{n_1}$ (2-2)

We have the following boundary conditions [14] :

$$D_{n_1}\left(\frac{d\Delta n_1}{dx}\right) = S_{n_1}\Delta n_1 \quad \text{for} \quad x = 0 \quad (2\text{-}3)$$

$$\Delta n_1 = 0 \quad \text{for} \quad x = x_1 \quad (2\text{-}4)$$

The expression of the electrons density photocreated in region 1 (window layer) can be written by :

$$\Delta n_1(x) = -\frac{\alpha_1 {L_{n_1}}^2 F(1-R)}{D_{n_1}\left(\alpha_1^2 {L_{n_1}}^2 - 1\right)} \times \left[e^{-\alpha_1 \cdot x} + \frac{\left(\frac{S_{n_1}L_{n_1}}{D_{n_1}} + \alpha_1 L_{n_1}\right)\cdot \mathrm{sh}\left(\frac{x-x_1}{L_{n_1}}\right) - e^{-\alpha_1 x_1}\left[\frac{S_{n_1}L_{n_1}}{D_{n_1}}\cdot \mathrm{sh}\left(\frac{x}{L_{n_1}}\right) + \mathrm{ch}\left(\frac{x}{L_{n_1}}\right)\right]}{\frac{S_{n_1}L_{n_1}}{D_{n_1}} sh\left(\frac{x_1}{L_{n_1}}\right) + ch\left(\frac{x_1}{L_{n_1}}\right)}\right] \quad (2\text{-}5)$$

The expression of the electrons photocurrent density is given by:

$$J_{n_1}(x) = -\frac{q\alpha_1 F(1-R)L_{n_1}}{\left(\alpha_1^2 {L_{n_1}}^2 - 1\right)} \times \left\{\frac{\left(\frac{S_{n_1}L_{n_1}}{D_{n_1}} + \alpha_1 L_{n_1}\right) ch\left(\frac{x-x_1}{L_{n_1}}\right) - e^{-\alpha_1 x_1}\left[\frac{S_{n_1}L_{n_1}}{D_{n_1}} ch\left(\frac{x}{L_{n_1}}\right) + sh\left(\frac{x}{L_{n_1}}\right)\right]}{\frac{S_{n_1}L_{n_1}}{D_{n_1}} sh\left(\frac{x_1}{L_{n_1}}\right) + ch\left(\frac{x_1}{L_{n_1}}\right)} - \alpha_1 L_{n_1} e^{-\alpha_1 x}\right\} \quad (2\text{-}6)$$

2-2. Calculation of the photocurrent in Region 2

In region 2, $x_1 \le x \le x_2$, the photocurrent is also an electron current, it results from the contribution of the regions 1 and 2, taking into account the interface effects characterized by a recombination velocity at the interface noted S_{n_2}. The continuity equation is given by:

$$\frac{d^2\Delta n_2}{dx^2} - \frac{\Delta n_2}{{L_{n_2}}^2} = \frac{-\alpha_2 F(1-R)e^{-\alpha_1 x_1}e^{-\alpha_2(x-x_1)}}{D_{n_2}} \quad (2\text{-}7)$$

With ${L_{n_2}}^2 = D_{n_2}\tau_{n_2}$ (2-8)

The boundary conditions are given by [15, 16] :

$$D_{n_2}\frac{d\Delta n_2}{dx} = S_{n_2}\Delta n_2 + D_{n_1}\frac{d\Delta n_1}{dx} \quad \text{for} \quad x = x_1 \quad (2\text{-}9)$$

$\Delta n_2 = 0$ for $x = x_2$ (2-10)

The solution of equation (2-7) is given by :

$$\Delta n_2(x) = -\frac{\alpha_2 {L_{n_2}}^2 F(1-R)\, e^{-\alpha_1 x_1}}{D_{n_2}\left(\alpha_2{}^2 {L_{n_2}}^2 - 1\right)} \times \left[e^{-\alpha_2 (x-x_1)} + \frac{\left(\frac{S_{n_2} L_{n_2}}{D_{n_2}} + \alpha_2 L_{n_2}\right) \cdot \mathrm{sh}\left(\frac{x-x_2}{L_{n_2}}\right) - e^{-\alpha_2 (x_2-x_1)} \left[\frac{S_{n_2} L_{n_2}}{D_{n_2}} \mathrm{sh}\left(\frac{x-x_1}{L_{n_2}}\right) + \mathrm{ch}\left(\frac{x-x_1}{L_{n_2}}\right)\right]}{\frac{S_{n_2} L_{n_2}}{D_{n_2}} sh\left(\frac{x_2-x_1}{L_{n_2}}\right) + ch\left(\frac{x_2-x_1}{L_{n_2}}\right)} \right] + \frac{\mathrm{sh}\left(\frac{x-x_2}{L_{n_2}}\right) \cdot J_{n_1}(x_1)}{\frac{qD_{n_2}}{L_{n_2}} \left\{ \frac{S_{n_2} L_{n_2}}{D_{n_2}} sh\left(\frac{x_2-x_1}{L_{n_2}}\right) + ch\left(\frac{x_2-x_1}{L_{n_2}}\right) \right\}} \quad (2\text{-}11)$$

The expression of the electrons photocurrent density in region 2, is :

$$J_{n_2}(x) = -\frac{q\alpha_2 F(1-R) L_{n_2} e^{-\alpha_1 x_1}}{\left(\alpha_2{}^2 {L_{n_2}}^2 - 1\right)} \times \left\{ \frac{\left(\frac{S_{n_2} L_{n_2}}{D_{n_2}} + \alpha_2 L_{n_2}\right) \mathrm{ch}\left(\frac{x-x_2}{L_{n_2}}\right) - e^{-\alpha_2 (x_2-x_1)} \left[\frac{S_{n_2} L_{n_2}}{D_{n_2}} ch\left(\frac{x-x_1}{L_{n_2}}\right) + sh\left(\frac{x-x_1}{L_{n_2}}\right)\right]}{\frac{S_{n_2} L_{n_2}}{D_{n_2}} sh\left(\frac{x_2-x_1}{L_{n_2}}\right) + ch\left(\frac{x_2-x_1}{L_{n_2}}\right)} - \alpha_2 L_{n_2} e^{-\alpha_2 (x-x_1)} \right\} + \frac{\mathrm{ch}\left(\frac{x-x_2}{L_{n_2}}\right) \cdot J_{n_1}(x_1)}{\frac{S_{n_2} L_{n_2}}{D_{n_2}} sh\left(\frac{x_2-x_1}{L_{n_2}}\right) + ch\left(\frac{x_2-x_1}{L_{n_2}}\right)} \quad (2\text{-}12)$$

2-3. Calculation of the photocurrent in the space charge region ($x_2 \le x \le x_2 + w$)

In the space charge region, we neglect the recombination of photocarriers. We distinguish two areas in this region :

- For $x_2 \le x \le x_2 + w_1$, the continuity equation of the photocreated electrons, is given by :

$$\frac{1}{q}\frac{dJ_{n_{w_1}}}{dx} + \alpha_2 F(1-R) e^{-\alpha_1 x_1} e^{-\alpha_2 (x-x_1)} = 0 \quad (2\text{-}13)$$

With $J_{n_{w_1}}(x_2) = 0$ (2-14)

The solution of equation (2-13) is :

$$J_{n_{w_1}}(x) = qF(1-R) e^{-\alpha_1 \cdot x_1} \left[e^{-\alpha_2 (x-x_1)} - e^{-\alpha_2 \cdot (x_2-x_1)} \right] \quad (2\text{-}15)$$

- For $x_2 + w_1 \le x \le x_2 + w_1 + w_2$, the continuity equation of the photocreated electrons, is given by :

$$\frac{1}{q}\frac{dJ_{n_{w_2}}}{dx} + \alpha_3 F(1-R) e^{-\alpha_1 x_1} e^{-\alpha_2 [(x_2+w_1)-x_1]} e^{-\alpha_3 [x-(x_2+w_1)]} = 0 \quad (2\text{-}16)$$

With $J_{n_{w_2}}(x_2 + w_1) = 0$ (2-17)

The solution of equation (2-16) is :

$$J_{n_{w_2}}(x) = qF(1-R) e^{-\alpha_1 x_1} e^{-\alpha_2 [(x_2+w_1)-x_1]} \left[e^{-\alpha_3 [x-(x_2+w_1)]} - 1 \right] \quad (2\text{-}18)$$

2-4. Calculation of the photocurrent in Region 3 and 4

The continuity equations in region 4 (substrate) and Region 3 (base) are respectively given by following equations (2-19) and (2-21):

$$\frac{d^2 \Delta p_4}{dx^2} - \frac{\Delta p_4}{L_{p_4}^2} = \frac{-\alpha_4}{D_{p_4}} F(1-R) e^{-\alpha_1 x_1} e^{-\alpha_2 [(x_2+w_1)-x_1]} \times e^{-\alpha_3 [x_3-(x_2+w_1)]} e^{\alpha_4 x_3} e^{-\alpha_4 x} \quad (2\text{-}19)$$

With $L_{p_4}^2 = D_{p_4} \tau_{p_4}$ (2-20)

$$\frac{d^2 \Delta p_3}{dx^2} - \frac{\Delta p_3}{L_{p_3}^2} = \frac{-\alpha_3}{D_{p_3}} F(1-R) e^{-\alpha_1 x_1} e^{-\alpha_2 [(x_2+w_1)-x_1]} \times e^{\alpha_3 (x_2+w_1)} e^{-\alpha_3 x} \quad (2\text{-}21)$$

With $L_{p_3}^2 = D_{p_3} \tau_{p_3}$ (2-22)

The holes density photocreated in the substrate is given by the solution of equation (2-19), it is written as:

$$\Delta p_4(x) = A'_4 e^{x/L_{P_4}} + B'_4 e^{-x/L_{P_4}} + K'_{P_4} e^{-\alpha_4 x} \quad (2\text{-}23)$$

With $K'_{P_4} = \frac{-\alpha_4 L_{p_4}^2 F(1-R) e^{[(\alpha_2-\alpha_1)x_1]} e^{[(\alpha_3-\alpha_2)(x_2+w_1)]} e^{[(\alpha_4-\alpha_3)x_3]}}{D_{p_4}\left(\alpha_4^2 L_{p_4}^2 - 1\right)}$ (2-24)

The solution of the equation (2-21) give the holes density photocreated in the base, it is written as:

$$\Delta p_3(x) = A'_3 e^{x/L_{P_3}} + B'_3 e^{-x/L_{P_3}} + K'_{P_3} e^{-\alpha_3 x} \quad (2\text{-}25)$$

With $K'_{P_3} = \frac{-\alpha_3 L_{p_3}^2 F(1-R) e^{[(\alpha_2-\alpha_1)x_1]} e^{[(\alpha_3-\alpha_2)(x_2+w_1)]}}{D_{p_3}(\alpha_3^2 L_{p_3}^2 - 1)}$ (2-26)

The constants A'_3, B'_3 , A'_4 and B'_4 are determined by using the following boundary conditions [17, 18]:

$$\Delta p_3(x) = 0 \quad \text{for} \quad x = x_2 + w \quad (2\text{-}27)$$

$$\Delta p_3(x) = \Delta p_4(x) \quad \text{for } x = x_3 \quad (2\text{-}28)$$

$$D_{p_3} \frac{d\Delta p_3}{dx} = D_{p_4} \frac{d\Delta p_4}{dx} \quad \text{for } x = x_3 \quad (2\text{-}29)$$

$$D_{p_4} \frac{d\Delta p_4}{dx} = -S_{p_4} \Delta p_4 \quad \text{for } x = H \quad (2\text{-}30)$$

From equations (2-23), (2-25) and the boundary conditions, we obtain the following matrix system :

$$\begin{bmatrix} X_{11} & X_{12} & 0 & 0 \\ X_{21} & X_{22} & X_{23} & X_{24} \\ X_{31} & X_{32} & X_{33} & X_{34} \\ 0 & 0 & X_{43} & X_{44} \end{bmatrix} \begin{bmatrix} A'_3 \\ B'_3 \\ A'_4 \\ B'_4 \end{bmatrix} = \begin{bmatrix} X'_1 \\ X'_2 \\ X'_3 \\ X'_4 \end{bmatrix} \quad (2\text{-}31)$$

With :

$X_{11} = e^{\frac{x_2+w}{L_{P_3}}}$; $X_{12} = e^{-\frac{x_2+w}{L_{P_3}}}$; $X_{21} = e^{\frac{x_3}{L_{P_3}}}$; $X_{22} = e^{-\frac{x_3}{L_{P_3}}}$; $X_{23} = -e^{\frac{x_3}{L_{P_4}}}$; $X_{24} = -e^{-\frac{x_3}{L_{P_4}}}$;

$X_{31} = -\frac{D_{p_3}}{L_{P_3}} e^{\frac{x_3}{L_{P_3}}}$; $X_{32} = \frac{D_{p_3}}{L_{P_3}} e^{-\frac{x_3}{L_{P_3}}}$; $X_{33} = \frac{D_{p_4}}{L_{P_4}} e^{\frac{x_3}{L_{P_4}}}$; $X_{34} = -\frac{D_{p_4}}{L_{P_4}} e^{-\frac{x_3}{L_{P_4}}}$;

$X_{43} = -e^{\frac{H}{L_{P_4}}} \left(\frac{D_{p_4}}{L_{P_4}} + S_{p_4}\right)$; $X_{44} = e^{-\frac{H}{L_{P_4}}} \left(\frac{D_{p_4}}{L_{P_4}} - S_{p_4}\right)$; $X'_1 = \frac{\alpha_3 L_{p_3}^2 F(1-R) e^{[(\alpha_2-\alpha_1)x_1]} e^{-\alpha_2 (x_2+w_1)}}{D_{p_3}(\alpha_3^2 L_{p_3}^2 - 1)}$;

$X'_2 = F(1-R) e^{[(\alpha_2-\alpha_1)x_1]} e^{[(\alpha_3-\alpha_2)(x_2+w_1)]} e^{-\alpha_3 x_3} \left[\frac{\alpha_3 L_{p_3}^2}{D_{p_3}(\alpha_3^2 L_{p_3}^2 - 1)} - \frac{\alpha_4 L_{p_4}^2}{D_{p_4}(\alpha_4^2 L_{p_4}^2 - 1)}\right]$;

$X'_3 = F(1-R) e^{[(\alpha_2-\alpha_1)x_1]} e^{[(\alpha_3-\alpha_2)(x_2+w_1)]} e^{-\alpha_3 x_3} \left[\frac{\alpha_3^2 L_{p_3}^2}{(\alpha_3^2 L_{p_3}^2 - 1)} - \frac{\alpha_4^2 L_{p_4}^2}{(\alpha_4^2 L_{p_4}^2 - 1)}\right]$;

$X'_4 = \frac{-\alpha_4 L_{p_4}^2 F(1-R) e^{[(\alpha_2-\alpha_1)x_1]} e^{[(\alpha_3-\alpha_2)(x_2+w_1)]} e^{[(\alpha_4-\alpha_3)x_3]} e^{-\alpha_4 H} [S_{p_4} - D_{p_4}\alpha_4]}{D_{p_4}(\alpha_4^2 L_{p_4}^2 - 1)}$

We propose a simple method for the determination of these constants. However, their expressions are too long, we will note them always A'_3, B'_3 , A'_4 and B'_4.

The equation (2-31) can be written as [19] :

$$\begin{bmatrix} 1 & 0 & 0 & 0 \\ L_{21} & 1 & 0 & 0 \\ L_{31} & L_{32} & 1 & 0 \\ 0 & 0 & L_{43} & 1 \end{bmatrix} \begin{bmatrix} U_{11} & U_{12} & 0 & 0 \\ 0 & U_{22} & U_{23} & U_{24} \\ 0 & 0 & U_{33} & U_{34} \\ 0 & 0 & 0 & U_{44} \end{bmatrix} \begin{bmatrix} A'_3 \\ B'_3 \\ A'_4 \\ B'_4 \end{bmatrix} = \begin{bmatrix} X'_1 \\ X'_2 \\ X'_3 \\ X'_4 \end{bmatrix} \quad (2\text{-}32)$$

With :

$U_{11} = X_{11}$; $U_{12} = X_{12}$;

$L_{21} = \frac{X_{21}}{U_{11}}$; $U_{22} = X_{22} - L_{21} \cdot U_{12}$; $U_{23} = X_{23}$; $U_{24} = X_{24}$;

$L_{31} = \frac{X_{31}}{U_{11}}$; $L_{32} = \frac{X_{32} - L_{31} \cdot U_{12}}{U_{22}}$; $U_{33} = X_{33} - L_{32} \cdot U_{23}$;

$U_{34} = X_{34} - L_{32} \cdot U_{24}$; $L_{43} = \frac{X_{43}}{U_{33}}$; $U_{44} = X_{44} - L_{43} \cdot U_{34}$

The resolution of Equation (2-32) is done in two steps. At first time, we solve the system:

ISSN: 2277-9655
Impact Factor: 4.116

$$\begin{bmatrix} 1 & 0 & 0 & 0 \\ L_{21} & 1 & 0 & 0 \\ L_{31} & L_{32} & 1 & 0 \\ 0 & 0 & L_{43} & 1 \end{bmatrix} \begin{bmatrix} Z_1 \\ Z_2 \\ Z_3 \\ Z_4 \end{bmatrix} = \begin{bmatrix} X'_1 \\ X'_2 \\ X'_3 \\ X'_4 \end{bmatrix}$$ (2-33), the solution of this problem is given by:

$Z_1 = X'_1 \; ; Z_2 = X'_2 - L_{21} \cdot Z_1 \; ; Z_3 = X'_3 - L_{31} \cdot Z_1 - L_{32} \cdot Z_2 \; ; Z_4 = X'_4 - L_{43} \cdot Z_3$

Secondly, we solve the following system:

$$\begin{bmatrix} U_{11} & U_{12} & 0 & 0 \\ 0 & U_{22} & U_{23} & U_{24} \\ 0 & 0 & U_{33} & U_{34} \\ 0 & 0 & 0 & U_{44} \end{bmatrix} \begin{bmatrix} A'_3 \\ B'_3 \\ A'_4 \\ B'_4 \end{bmatrix} = \begin{bmatrix} Z_1 \\ Z_2 \\ Z_3 \\ Z_4 \end{bmatrix}$$ (2-34), the solution is given by:

$B'_4 = \frac{Z_4}{U_{44}} \; ; A'_4 = \frac{Z_3 - U_{34} \cdot B'_4}{U_{33}} \; ; B'_3 = \frac{Z_2 - U_{23} \cdot A'_4 - U_{24} \cdot B'_4}{U_{22}} \; ; \; A'_3 = \frac{Z_1 - U_{12} \cdot B'_3}{U_{11}}$

The expression of the holes photocurrent density is given by :

$$J_{p_3}(x) = -qD_{p_3}\left[\frac{A'_3}{L_{P_3}} e^{x/L_{P_3}} - \frac{B'_3}{L_{P_3}} e^{-x/L_{P_3}} - \alpha_3 K'_{P_3} e^{-\alpha_3 x}\right]$$ (2-35)

2-5. calculation of result photocurrent

The result photocurrent is constant. His expression results from the contribution of the different regions of the structure, it can be written as [20]:

$$J_{ph} = J_{n_2}(x_2) + J_{n_{w_1}}(x_2 + w_1) + J_{n_{w_2}}(x_2 + w) + J_{p_3}(x_2 + w)$$ (2-36)

The internal quantum efficiency is given by :

$\eta = \left|\frac{J_{ph}}{J_0}\right|$ (2-37), with $J_0 = qF(1 - R)$ [21]

2-6. Two and three layers model : p/n ; p⁺/p/n ; p/n/n⁺

The results which are appropriate for the other models (2 and 3 layers model) can be deduced easily from previous calculations:

- in the case of the model p⁺/p/n, it is just sufficient to take $\alpha_4 = \alpha_3$ and to remove the substrate (region 4) on Figures 2 and 3 ;
- for the model p/n/n⁺, it is just sufficient to establish $\alpha_1 = 0$; $x_1 = 0$ and to remove the window layer (region 1) on Figures 2 and 3;
- for the structure p/n, we take $\alpha_1 = 0$; $x_1 = 0$; $\alpha_4 = \alpha_3$ and remove the window layer (region 1) and the substrate (region 4) on Figures 2 and 3.

These different conditions of passage are shown on Figure 4.

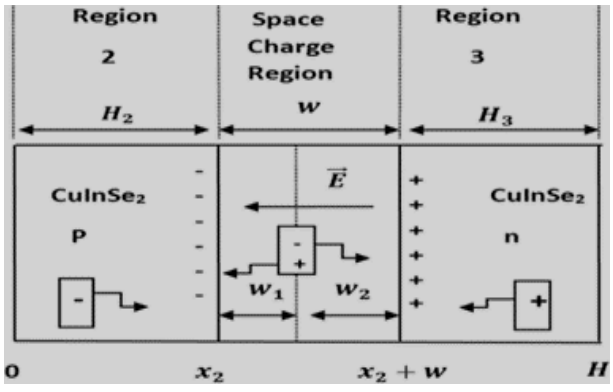

(a). We take $\alpha_1 = 0$; $x_1 = 0$; $\alpha_4 = \alpha_3$ and remove the window layer (region 1) and the substrate (region 4)

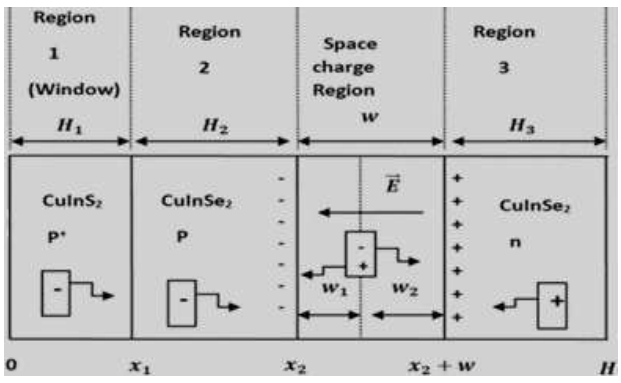

(b). We take $\alpha_4 = \alpha_3$ and remove the substrate (region 4)

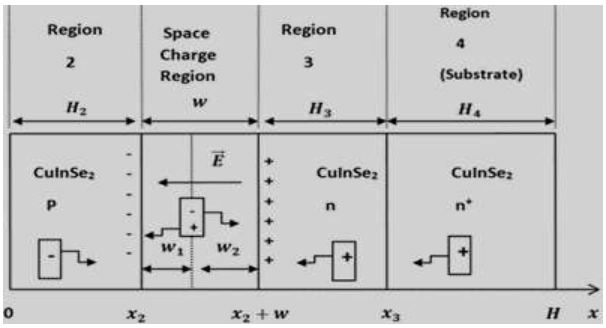

Figure 4. diagrams of the structure for the other models :

(a) : $CuInSe_2(p)/CuInSe_2(n)$

(b) : $CuInS_2(p^+)/ CuInSe_2(p)/CuInSe_2(n)$

(c) : $CuInSe_2(p)/CuInSe_2(n)/CuInSe_2(n^+)$

(c). We take $\alpha_1 = 0$; $x_1 = 0$ and remove the window layer (region 1)

RESULTS AND DISCUSSION

In this part we present a simulation of the theoretical models developed. We study the effects of geometrical parameters on the performance of each model. We compare the different results and evaluate the best short-circuit photocurrent. We note H_i as the thickness of the region i.

3-1. Comparative study of the internal quantum efficiency

On Figure 5 a) we compare the internal quantum efficiency of the homojunction with window layer deposited on substrate ($CuInS_2(p^+)/CuInSe_2(p)/CuInSe_2(n)/CuInSe_2(n^+)$) to the internal quantum efficiency of the other models : the homojunction with window layer ($CuInS_2(p^+)/CuInSe_2(p)/CuInSe_2(n)$), the homojunction deposited on substrate ($CuInSe_2(p)/CuInSe_2(n)/CuInSe_2(n^+)$) and the homojonction ($CuInSe_2(p)/CuInSe_2(n)$). To study the effects of the substrate and the base, we fixed the thickness of the region 2 at 0.1 µm. However, we note the effect of the substrate in the range of low energies (1.04 eV < E <1.4 eV). In this range (1.04 eV < E <1.4 eV), the 4 layers model ($p^+/p/n/n^+$) gives the best internal quantum efficiency followed by the models with 3 layers ($p/n/n^+$ and $p^+/p/n$). The signal given by the model $p/n/n^+$ is greater than that given by the model $p^+/p/n$ only for photon energies lower than 1.2 eV. The model with 2 layers (p/n) gives the lowest performance. For higher energies (E> 1.57 eV) the spectral responses given by the models $p^+/p/n/n^+$ and $p^+/p/n$ are identical. We observe the same phenomenon for the models $p/n/n^+$ and p/n.

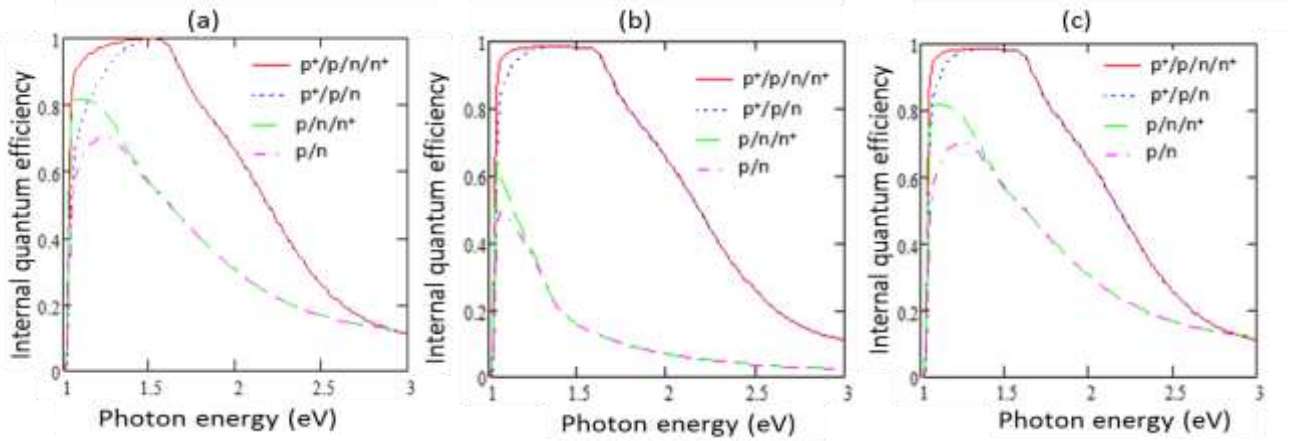

Figure 5. Internal quantum efficiency vs. Photon energy :Comparative Study of the different models ($s_{n_1}=2\times10^7\ cm.s^{-1}$; $H_1 = 0.1\ \mu m$; $L_{n_1}= 0.5\ \mu m$; $H_2 = 0.1\ \mu m$ (a ; c : p/n and $p/n/n^+$) and 0.5 µm (b ; c : $p^+/p/n$ and $p^+/p/n/n^+$); $L_{n_2}= 3\ \mu m$; $s_{n_2}=2\times10^3 cm.s^{-1}$; $s_{p_3}=2\times10^7 cm.s^{-1}$ (p/n) ; $L_{p_3}= 3\ \mu m$ ($p/n/n^+$ and $p^+/p/n/n^+$) and 0.5 µm (p/n and $p^+/p/n$) ; $H_3 = 5\ \mu m$; $s_{p_4}=2\times10^7 cm.s^{-1}$; $L_{p_4}= 0.5\ \mu m$; $W_1= 0.05\ \mu m$; $W_2= 0.05\ \mu m$; $W= 0.1\ \mu m$; $H = 100\ \mu m$)

On Figure 5 b) we increased the thickness of the region 2 at 0.5 µm. The structure $p^+/p/n/n^+$ always gives the best spectral response. Its signal is slightly higher than the signal given by the model $p^+/p/n$ in a more limited energy range

(1.04 eV< E <1.3 eV). For radiation energies greater than 1.3 eV (E > 1.3 eV), the spectral response is identical for these two models ($p^+/p/n/n^+$ and $p^+/p/n$) and remains practically high compared to the models $p/n/n^+$ and p/n. We note that, the increase of the thickness of the region 2, enhances the internal quantum efficiency in the case of the homojunction with window layer deposited on substrate ($p^+/p/n/n^+$) and the homojunction with window layer ($p^+/p/n$). A drop of the internal quantum efficiency is observed in the case of the homojunction deposited on substrate ($p/n/n^+$) and the homojunction (p/n). These results show the effects of the losses of carriers by recombination on the front surface. In the case of the models with 4 layers and 3 layers with window layer, the window layer (region 1) reduces losses of carriers at the interface region 1 – region 2 ($S_{n_2} = 2 \times 10^3$ cm.s^{-1}) and allows the majority of carriers to diffuse towards the collecting area (space charge region). For the homojunction deposited on substrate and the homojunction, the losses of carriers on the front surface (region 2) are important ($S_{n_2} = 2 \times 10^7$ cm.s^{-1}). Some carriers diffuse towards the surface and cause the decrease of the internal quantum efficiency.

On figure 5 c) we reduced the thickness of the region 2 at 0.1 µm for the structures $p/n/n^+$ and p/n. We note an enhancement of the internal quantum efficiency for these two models by reducing the contribution of region 2.

However, the internal quantum efficiency is dominated by the homojunction with window layer deposited on substrate ($CuInS_2(p^+)/CuInSe_2(p)/CuInSe_2(n)/CuInSe_2(n^+)$) followed by the homojunction with window layer ($CuInS_2(p^+)/CuInSe_2(p)/CuInSe_2(n)$). the lowest signal is given by the homojunction ($CuInSe_2(p)/CuInSe_2(n)$).

The decrease of the signal observed in the range of elevated energies (E > 1.57 eV) on each graph is due by the losses of carriers by recombination on the front surface (illuminated surface).

3-2. Study of the structure $p^+/p/n/n^+$ (Region 1 / Region 2 / Region 3 / Region 4) under monochromatic illumination

In this part, we consider the structure $p^+/p/n/n^+$. We study, in the case of a monochromatic illumination, the graphs of the generation rate, of the densities of minority carriers and result photocurrent versus junction depht (x). We maintain the values used on Figure 5 c). We consider radiation energies ranging from 1.04 eV (λ = 1.192 µm) to 3.1 eV (λ = 0.4 µm).

3-2-a. generation rate under monochromatic illumination

Figures 6 show the generation rate versus junction depht (x) for different monochromatic illumination.

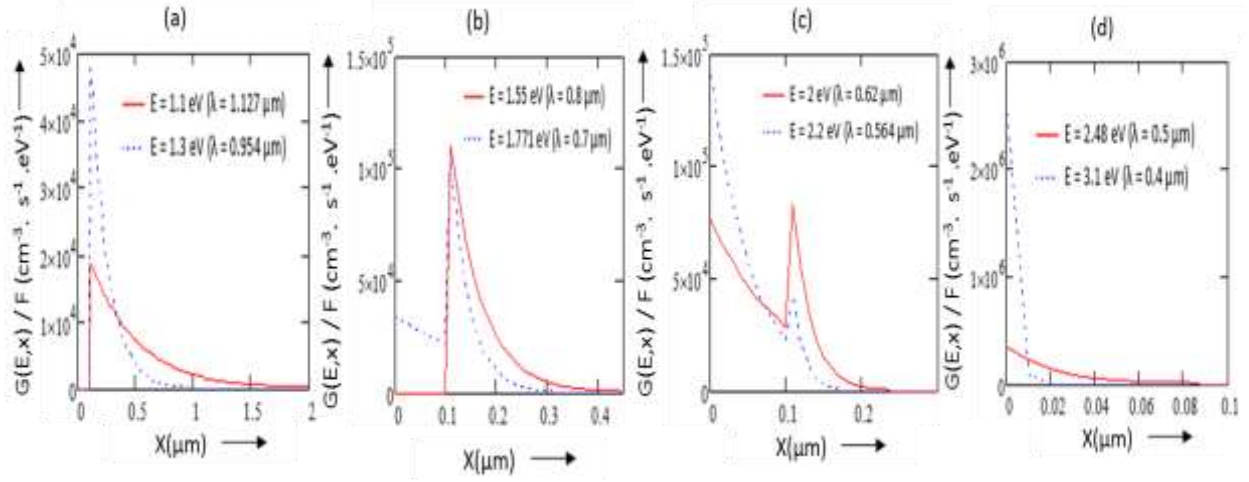

Figure 6. generation rate vs. junction depth (x) under monochromatic illumination

In the range of low energies (1.04 < E < 1.3 eV), the photons reach the back regions (base and substrate: X > 0.7 µm) (Figure 6 a). The effect of the substrate is important in this energy range.

In the range of elevated energies (E > 1.3 eV), the photons are absorbed on a thin thickness. The frontal regions (window layer, region 2 and space charge region : X < 0.7 µm) absorb the majority of these photons (Figures 6b and 6c) and the effect of the window layer (X< 0.1 µm) becomes significant.

For radiation energies more elevatead than the energy band gap of the window layer, most of photons are absorbed by the front layer (Figure 6d).

ISSN: 2277-9655
Impact Factor: 4.116

3-2-b. densities of minority carriers under monochromatic illumination

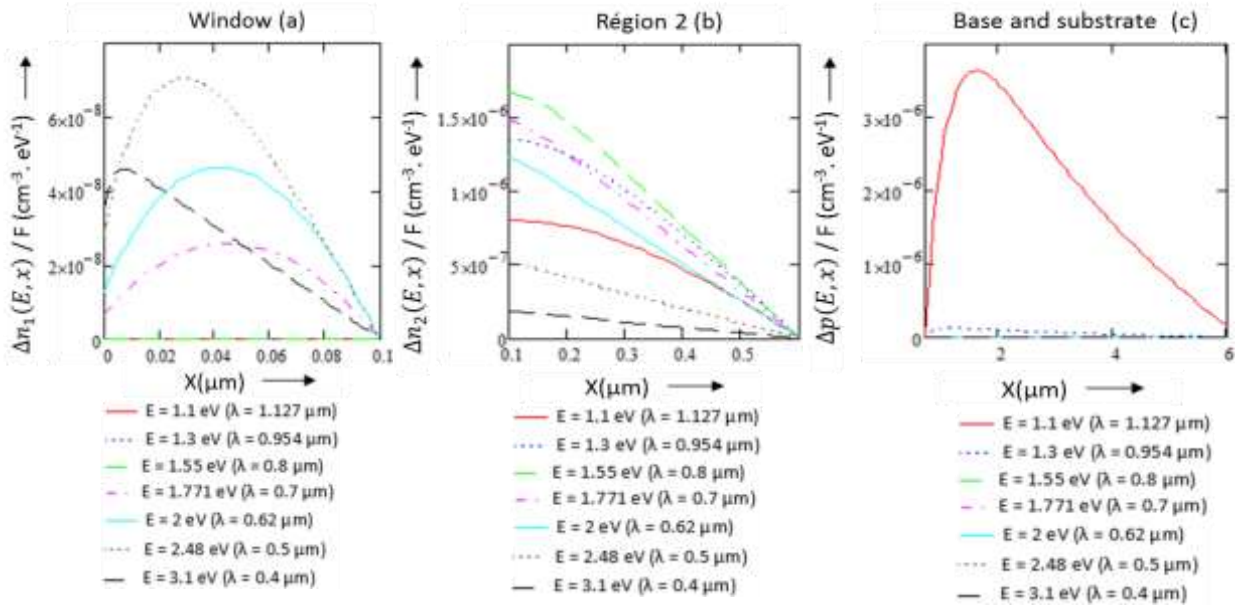

Figure 7. density of minority carriers photocreated vs. junction depth (x) under monochromatic illumination: a) density of electrons in region 1 (window) ; b) density of electrons in region 2; c) density of holes in regions 3 and 4 (base and substrate)

On figure 7 a), we represent, for different illuminations, the density of electrons photocreated in the window layer (0 µm < X < 0.1 µm). Only radiation energies greater than the energy band gap of the window layer (E> 1.57 eV) are absorbed by this region. Each graph is characterized by two steps.

A first step where the photocarriers density increases with the thickness. In this step the minority carriers diffuse toward the front surface of the window layer where they disappear by recombination phenomenon.

A second step where the photocarriers density decreases with the thickness. They diffuse toward the region 2, their collect depends on the interface effects between regions 1 and 2.

Figure 7 b) shows the density of electrons photocreated in region 2 (0.1 µm < X < 0.6 µm). In this region the density of electrons results from the contribution of the regions 1 (E > 1.57 eV) and 2 (1.04 eV < E < 2 eV). For each radiation, the density of photocarriers decreases towards the collecting region (space charge region : 0.6 µm < X < 0.7 µm). This phenomenon means that the losses of carriers at the interface are reduced by the window layer ($S_{n_2} = 2 \times 10^3$cm.s^{-1}) and the majority of photocarriers (electrons) diffuses towards the space charge region where they will be collected.

Figure 7 c) shows the density of holes photocreated in the rear area (base and substrate : X > 0.7 µm). These regions absorb photons of low energies (1.04 eV <E <1.3 eV). The photons of high and medium energies (E> 1.3 eV) are mostly absorbed by the frontal layers (window layer, region 2 and space charge region). The graph of the holes density presents two steps.

A first step where the holes density increases with the thickness. In this step they diffuse toward the space charge region where they will be collected.

A second step where the holes density decreases with the thickness. The photocarriers (holes) diffuse toward the back surface, they will be lost by recombination phenomenon.

3-2-c. photocurrent densities of minority carriers under monochromatic illumination

On Figure 8 a) we represent, for each radiation, the densities of electrons photocurrent versus junction depht in the frontal layers (window layer, region 2 and space charge region : X < 0.7 µm). For radiation energies greater than the energy band gap of the window layer (E >1.57 eV), the graph of the electrons photocurrent presents a negative small portion (X < 0.02 µm) modelling the losses of carriers at the front surface ($S_{n_1} = 2 \times 10^7$ cm.s^{-1}). We obtain the best

densities of electrons photocurrent for radiation energies less than the energy band gap of the window layer (E < 1.57 eV).

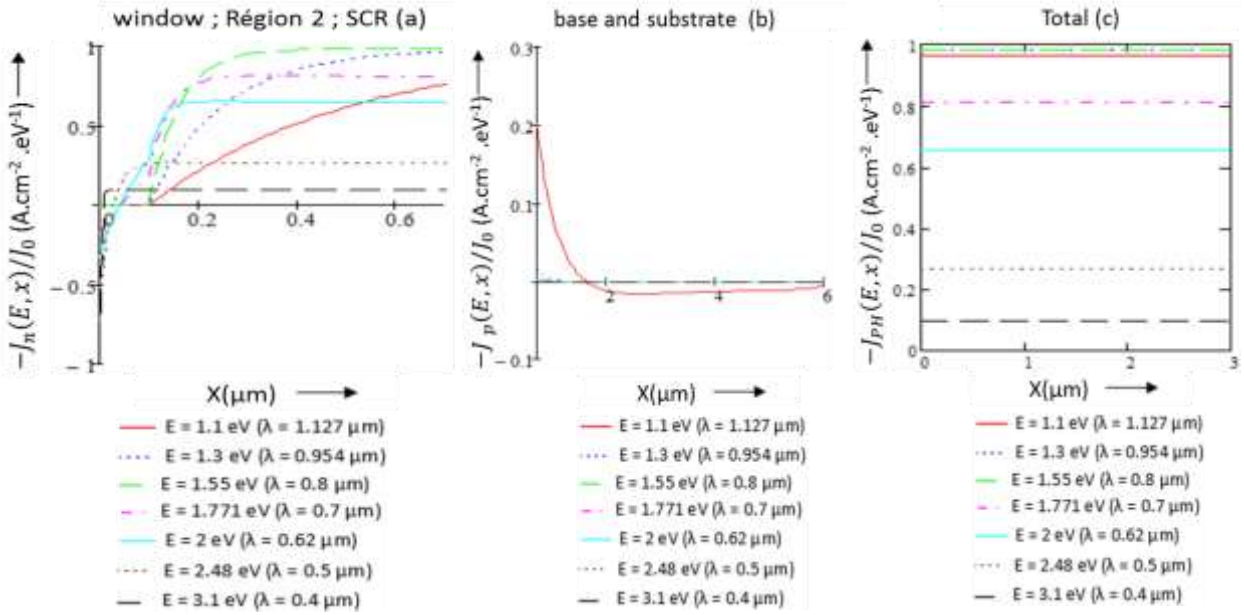

Figure 8. photocurrent density of minority carriers photocreated vs. junction depth (x) under monochromatic illumination : a) photocurrent density of electrons (window - Région 2 – space charge region); b) photocurrent density of holes (base – substrate) ; c) result photocurrent density

Figure 8 b) shows the densities of holes photocurrent in the rear regions (base and substrate : X > 0.7 µm). The photocurrent of holes is essentially due by the photons of low energies (1.04 < E < 1.3 eV) wich reach the base or the substrate. The photons of elevated energies (E > 1.3 eV) being absorbed by the frontal regions (window layer, region 2 and space charge region : X < 0.7 µm). However we note that the density of the hole photocurrent for the energy radiation E = 1.1 eV (λ = 1.127 µm) presents two parts. A positive part (0.7 µm < X < 1.8 µm) due to the diffusion of minority carriers towards the collecting region (space charge region : 0.6 µm < X < 0.7 µm). A negative part (X > 1.8 µm) modelling the losses of the minority carriers; it is due to their diffusion towards the back surface.

Figure 8 c) shows the total density of photocurrent versus junction depth, it results from the contribution of the electrons and holes photocurrent. His expression is given by the equation (2-36). The photons absorbed mostly by the region 2 and the space charge region (1.3 eV < E < 1.57 eV) give the best response. The losses of carriers by recombination are reduced in these regions (see the parameters used in Figure 5 c) for the model $p^+/p/n/n^+$. The photons of low energies (1.04 eV <E<1.3 eV), absorbed mostly by the rear regions (base and substrate) give an important photocurrent. The presence of the substrate allows to reduce the impurities in the base by reducing the doping level (increase of the diffusion length) and then the losses of carriers are reduced in the base. The photons absorbed by the window layer (E>1.57 eV) give a photocurrent affected by the losses of carriers due to the dislocation of the surface at the front layer.

3-3. Theoretical calculation of the short-circuit photocurrent under solar spectra AM 0, AM 1.5, AM 1

On figure 9 a) we represent three solar spectra of reference versus photon wave length [22], allowing to evaluate the theoretical short-circuit photocurrent. Figure 9 b) represents the three solar spectra of reference versus photon energy, it is obtained using the equation (3-1).

$$F\ (cm^{-2}.s^{-1}.eV^{-1}) = \Phi\ (cm^{-2}.s^{-1}.\mu m^{-1}) \times \frac{1.24}{E^2} \quad (3\text{-}1)$$

F and Φ represent photon flux.

ISSN: 2277-9655
Impact Factor: 4.116

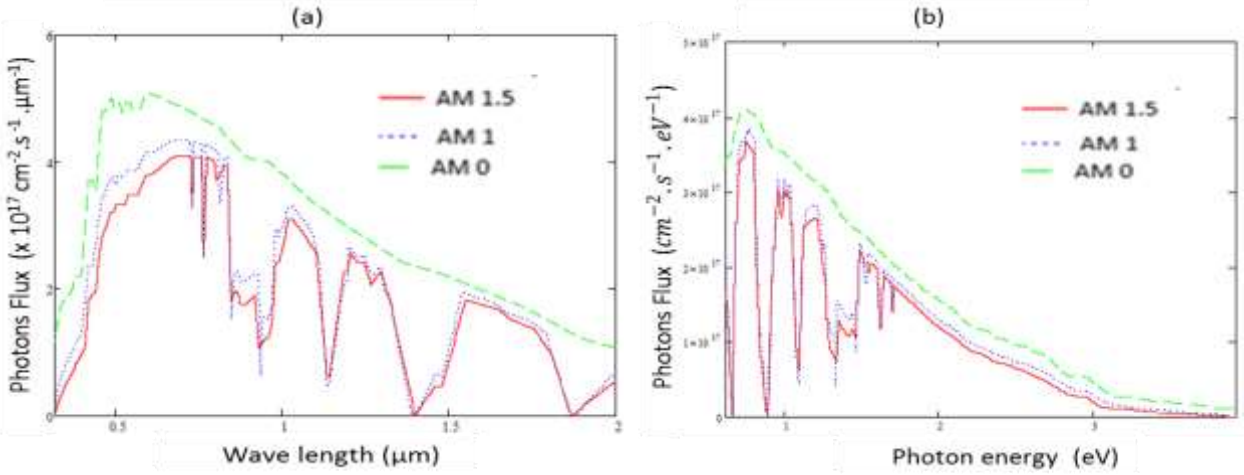

Figure 9. a) photon flux vs. photon wave length [22] ; b) photon flux vs. photon energy

Figures 10 a) and 10 b) respectively represent the photocurrent densities (see equation 2-36) versus photon energy for the solar spectra AM 0 and AM 1.5 of the different models ($p^+/p/n/n^+$; $p^+/p/n$; $p/n/n^+$; p/n) studied on figure 5 c).

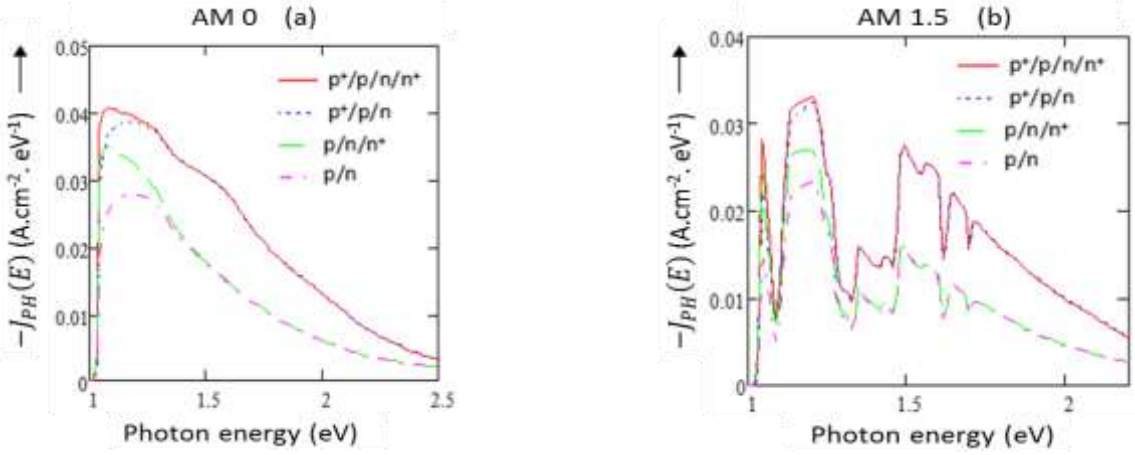

Figure 10. Result photocurrent density vs. photon energy: a) AM 0 ; b) AM 1.5

Calculation of the short-circuit photocurrent J_{sc} on the solar spectral ranging from 1 eV to 3 eV is given by $\int_1^3 -J_{ph}\,(E)dE$. For this calculation, we propose a numerical integration method. We use the Newton quadrature.
We note:

$$J_{sc} = -\int_1^3 J_{ph}\,(E)dE \approx -\frac{\delta E}{2}\left[J_{ph}(E_1) + J_{ph}(E_{m+1}) + 2\sum_{i=2}^{m} J_{ph}(E_i)\right] \quad (3\text{-}2)$$

With: $E \in [1\ eV\ , 3\ eV]$; $E_1 = 1\ eV$; $E_{m+1} = 3$ eV; $\delta E = \frac{E_{m+1} - E_1}{m}\ eV$

$E_{i+1} = (E_1 + i \cdot \delta E)\ eV \ \ ; i : 1 \ldots m$

For this calculation, we pose $m = 100$ and obtain the following theoretical short-circuit photocurrent :

	$p^+/p/n/n^+$	$p^+/p/n$	$p/n/n^+$	p/n
AM 0	32 mA.cm^{-2}	31 mA.cm^{-2}	21 mA.cm^{-2}	19 mA.cm^{-2}
AM 1.5	21 mA.cm^{-2}	21 mA.cm^{-2}	14 mA.cm^{-2}	13 mA.cm^{-2}

3-4. Study of the structure $p^+/p/n/n^+$ (Region 1 / Region 2 / Region 3 / Region 4) under polychromatic illumination (AM 0, AM 1.5, AM 1)

A relation similar to the expression (3-2) allows to obtain, the graphs of the generation rate, of the densities of minority carriers and the short-circuit photocurrent versus junction depth under AM 0, AM 1 and AM 1.5 solar spectra. We always consider the structure $p^+/p/n/n^+$ and maintain the values used on Figure 5 c).

3-4-a. generation rate under polychromatic illumination (AM 0, AM 1.5, AM 1)

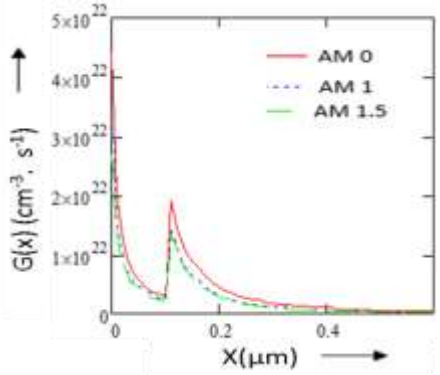

Figure 11. generation rate vs. junction depth (x) under polychromatic illumination

Figure 11 shows the generation rate under AM 0, AM 1 and AM 1.5 solar spectra. Photons are absorbed mostly by the front layers (window layer for X< 0.1 μm , region 2 and space charge region for 0.1 μm < X < 0.7 μm). This low penetration depth of the photons is due to the high photonic absorption coefficients of the used materials ($CuInSe_2$ and $CuInS_2$).

The considerable absorption of the photons by the window layer (X< 0.1 μm) reduces the short-circuit photocurrent. This is due by the losses of carriers by recombination at the front surface of this region.

3-4-b. densities of minority carriers under polychromatic illumination (AM 0, AM 1.5, AM 1)

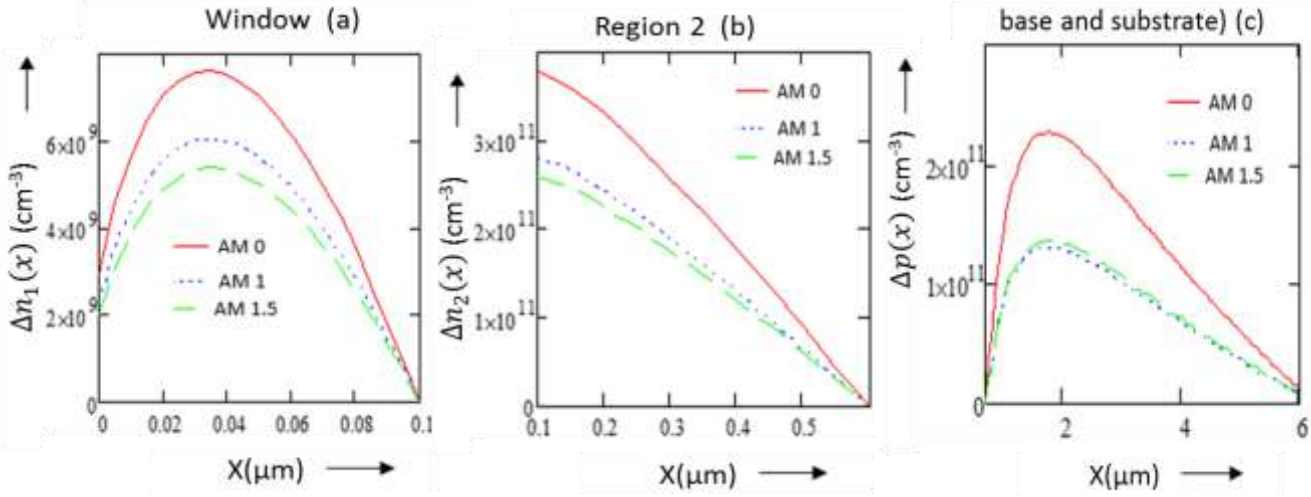

Figure 12. density of minority carriers photocreated vs. junction depth (x) under polychromatic illumination: a) density of electrons in region 1 (window) ; b) density of electrons in region 2 ; c) density of holes in regions 3 and 4 (base and substrate)

Figure 12 a) shows the total density of electrons photocreated in the window layer (X< 0.1 μm) versus junction depth under AM 0, AM 1 and AM 1.5 solar spectra. As noted in the case of monochromatic illumination, each curve presents a first step modeling losses of carriers at the front surface (the density of electrons increases with the thickness) and a second step modeling the diffusion of minority carriers towards the region 2 (the density of electrons decreases with the thickness).

Figure 12 b) shows the total density of electrons photocreated in region 2 (0.1 µm < X < 0.6 µm) versus junction depth under AM 0, AM 1 and AM 1.5 solar spectra. Each curve presents only one step where the density of electrons decreases with the thickness. Losses at the interface region 1 – region 2 are reduced by the window layer ($S_{n_2} = 2 \times 10^3$ cm.s^{-1}). The photocreated electrons diffuse mainly towards the space charge region (0.6 µm < X < 0.7 µm). Their collect depends to their diffusion length, it must be greater than the thickness of the region 2 ($L_{n_2} > H_2$) [23].

Figure 12 c) shows the total density of holes photocreated in the base (0.7 µm < X < 5.7 µm) and the substrate (X > 5.7µm) versus junction depth under AM 0, AM 1 and AM 1.5 solar spectra. The portion of the holes photogenerated near the space charge region (0.6 µm < X < 0.7 µm) and having a sufficient diffusion length is collected. This phenomenon explains the gradient of concentration observed near the space charge region (0.7 µm < X < 2 µm). The step where the photocarriers density decrease with the thickness (X > 2 µm) is due to the diffusion of the holes toward the back surface. These carries are lost by recombination phenomenon.

3-4-c. photocurrent densities of minority carriers under polychromatic illumination (AM 0, AM 1.5, AM 1)

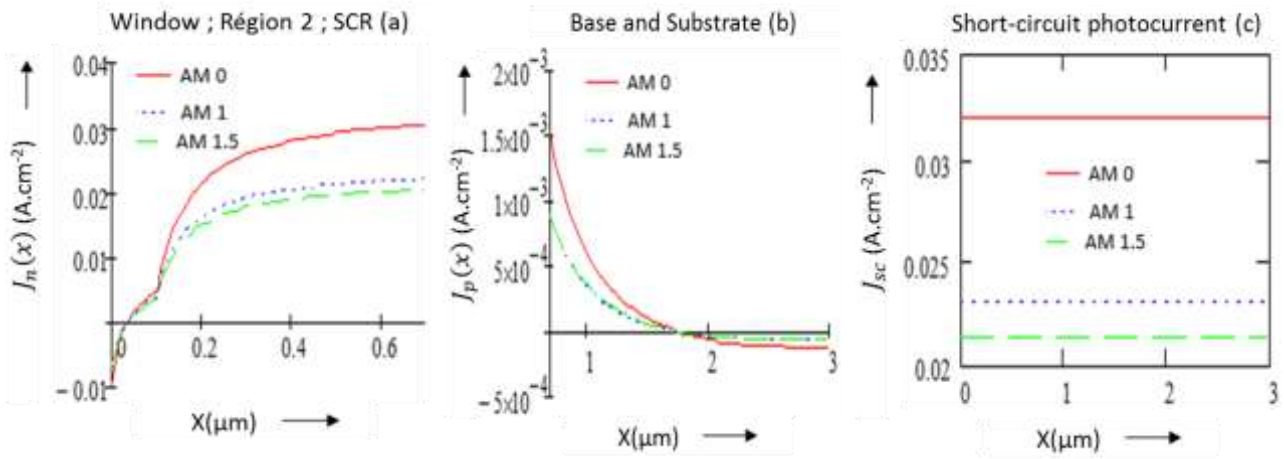

Figure 13. photocurrent density of minority carriers photocreated vs. junction depth(x) under polychromatic illumination: a) photocurrent density of electrons (window - Région 2 – space charge region); b) photocurrent density of holes (base – substrate) ; c) : result photocurrent density

Figures 13 a) and 13 b) represent respectively the photocurrent density of the electrons at the frontal regions (window, region 2 and the space charge region : X < 0.7 µm) and the holes at the rear regions (base and substrate : X > 0.7µm). The negative portion observed on each graph shows the losses of photocurrent. The diffusion of the photocarriers towards the depletion region is modelled by the positive portion observed on each graph. The photocurrent increases near the space charge region modeling a high collect of minority carriers. The short-circuit photocurrent resulting from the contribtion of electrons and holes photocurrent is shown in Figure 13 c).

However the short-circuit photocurrent can be enhanced by reducing losses at the front surface of the window layer, this is possible by depositing a second window layer. So for the model p$^+$/p/n shown in Figure 5 c), by fixing the recombination velocity $S_{n_1} = 2 \times 10^5$ cm.s^{-1}, the short-circuit photocurrent increases from 31 mA.cm^{-2} to 39 mA.cm^{-2} for AM 0 spectrum and from 21 mA.cm^{-2} to 27 mA.cm^{-2} for AM 1.5 spectrum. Figures 14 represent the graphs of the corresponding photocurrent densities. Figures 14 a) and b) show respectively the density of photocurrent versus photon energy and the short-circuit photocurrent versus junction depth for AM 0, AM 1 and AM 1.5 solar spectra. Figure 14 c) shows the short-circuit photocurrent and the density of electrons and holes photocurrent versus junction depth for AM 1.5 solar spectrum.

ISSN: 2277-9655
Impact Factor: 4.116

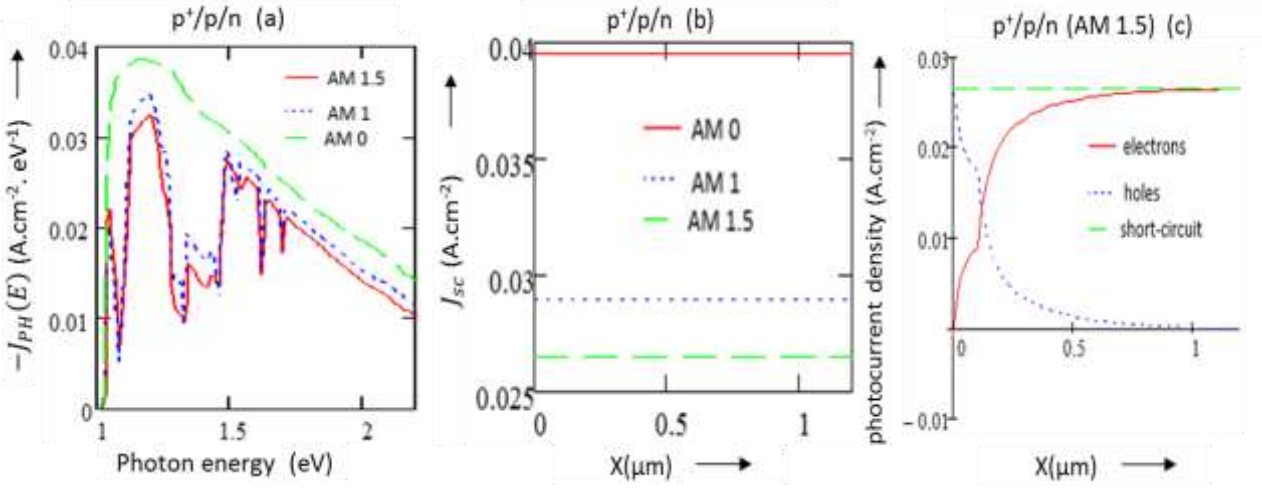

Figure 14 : photocurrent density of minority carriers photocreated under polychromatic illumination : a) result photocurrent density vs. photon energy; b) Short-circuit photocurrent vs. junction depth (x) ; c) electrons, holes and short-circuit photocurrent vs. junction depth (x)

CONCLUSION

In this work we have compared the performances of solar cells based on $CuInSe_2$ by studying the following models: homojunction ($CuInSe_2$(p)/$CuInSe_2$(n)), homojunction deposited on substrate ($CuInSe_2$(p)/$CuInSe_2$(n)/$CuInSe_2$(n^+)), homojunction with window layer ($CuInS_2$(p^+)/$CuInSe_2$(p)/$CuInSe_2$(n)), homojunction with window layer deposited on substrate ($CuInS_2$(p^+)/$CuInSe_2$(p)/$CuInSe_2$(n)/ $CuInSe_2$(n^+)) . The window layer allows to enhance significantly the spectral response for radiation energies lower than his energy band gap (1.04 < E <1.57 eV) for the structures $p^+/p/n/n^+$ and $p^+/p/n$. The presence of the substrate enhances the internal quantum efficiency in the range of low energies (1.04 < E <1.4 eV). The structure $p^+/p/n/n^+$ gives the best signal. His internal quantum efficiency varies from 85 to 100% for photons energies less than the energy band gap of the window layer (1.04 < E <1.57 eV). This efficiency decreases for photons energies higher than the energy band gap of the window layer (E > 1.57 eV), it is due by the losses of carriers caused by the absorption of the front layer (window).

We have studied, in the case of the structure $p^+/p/n/n^+$, the generation rate, the densities of photocarriers and photocurrent for a monochromatic and polychromatic illumination (AM 0, AM 1 and AM 1.5 spectrum). It allowed to analyze in detail the effects of the different layers and the geometrical and electrical parameters on the photocurrent, and explains the signal of the internal quantum efficiency.

The theoretical short circuit photocurrent calculated in this work (21 – 27 $mA.cm^{-2}$ under AM 1.5 spectrum for the models $p^+/p/n/n^+$ and $p^+/p/n$), remains in the range of the values reported in the literature. This current can be enhanced by using a wide band gap window layer or reducing losses in the window.

NOMENCLATURE

β : n (electrons) or p (holes) ; i : region (1, 2, 3 or 4)

α_i : Absorption coefficient of region i (cm^{-1})

F : Incident photons flux ($cm^{-2}.s^{-1}.eV^{-1}$) (or ($cm^{-2}.s^{-1}$))

Φ : Incident photons flux ($cm^{-2}.s^{-1}.\mu m^{-1}$) (or ($cm^{-2}.s^{-1}$))

R : Reflection coefficient ($R = 0.2$)

τ_{β_i} : Lifetime of free electrons or holes photocreated in region i (μs)

$\Delta\beta_i(x)$: Density of free electrons or holes photocreated in region i at the point of x coordinate ($cm^{-3}.eV^{-1}$) (or (cm^{-3}))

$J_{\beta_i}(x)$: Photocurrent density of free electrons or holes photocreated in region i at the point of x coordinate ($A.cm^{-2}\ eV^{-1}$) (or ($A.cm^{-2}$))

J_{ph} : Total density of photocurrent $(A.cm^{-2}.eV^{-1})$

J_{sc} : short circuit current$(A.cm^{-2})$

D_{β_i} : Diffusion coefficient of free electrons or holes photocreated in region i $(cm^2.s^{-1})$ $(D_{n_1} = D_{n_2} = 15.41\ cm^2.s^{-1}\ and\ D_{p_3} = D_{p_4} = 1.28\ cm^2.s^{-1})$

L_{β_i} : Diffusion length of free electrons or holes photocreated in region i (μm)

S_{β_i} : Recombination velocity on the surface (or to the interface) of region i $(cm.s^{-1})$

H : Thickness of the structure (μm)

H_i : Thickness of the region i (μm)

w_i : Thickness of the region i of the space charge region (SCR) (μm)

q : Elementary charge $(1.602 \times 10^{-19} C)$

$\chi_{CuInSe2}$: Electron affinity of $CuInSe_2$

χ_{CuInS2} : Electron affinity of $CuInS_2$

$E_{gCuInSe2}$: Energy band gap of $CuInSe_2$

$E_{gCuInS2}$: Energy band gap of $CuInS_2$

REFERENCES

1. S. Khelifi et A. Belghachi, '' Le Rôle de la Couche Fenêtre dans les Performances d'une Cellule Solaire GaAs'', Rev. Energ. Ren. Vol.7 (2004) 13-21.
2. M.V. Yakushev , A.V. Mudryi, V.F. Gremenok, V.B. Zalesski, P.I. Romanov, Y.V. Feofanov, R.W. Martin, R.D. Tomlinson, ''Optical properties and band gap energy of $CuInSe_2$ thin films prepared by two-stage selenization process'', Journal of Physics and Chemistry of Solids, 2003, Volume 64, Pages 2005–2009
3. Ariswan, G. El Haj Moussa, F. Guastavino, C. Llinares,'' Band gap of $CuInSe_2$ thin films fabricated by flash evaporation determined from transmission data'' Journal of Materials Science Letters, Volume 21, pp 215-217
4. S. B. Zhang, Su-Huai Wei, and Alex Zunger, '' Stabilization of Ternary Compounds via Ordered Arrays of Defect Pairs'', Phys. Rev. Lett, 1997, vol. 78, 4059
5. Abazović Nadica D., Jovanović Dragana J., Stoiljković Milovan M., Mitrić Miodrag N., Ahrenkil Phillip S., Nedeljković Jovan M., Čomor Mirjana I., ''Colloidal-chemistry based synthesis of quantized CuInS2/Se2 nanoparticles'', Journal of the Serbian Chemical Society, 2012, Volume 77, Pages: 789-797
6. Subba Ramaiah Kodigala, ''$Cu(In_{1-x}Ga_x)se_2$ based thin solar cells'', 2010, Volume 35, Academic Press, ELSEVIER.Inc, p. 16.
7. T. Loher, W. Jaegermann, C. Pettenkofer, ''Formation and electronic properties of the $CdS/CuInSe_2$ (011) heterointerface studied by synchrotron-induced photoemission'', J. Appl. Phys. 77 (1995) 731.
8. H. Hahn, G. Frank, W. Klinger, A.D. Meyer, G. Stroger, '' Über einige ternäre Chalkogenide mit Chalcopyritestruktur'', Z. Anorg. Aug. Chem. 271 (1953) 153.
9. M. Robbins, V.G. Lambrecht Jr., '' Preparation and some properties of materials in systems of the type $M^IM^{III}S_2$ / $M^IM^{III}Se_2$ where M^I = Cu, Ag and M^{III} = Al, Ga, In'', Mater. Res. Bull. 8 (1973) 703.
10. I.V. Bodnar, B.V. Korzun, A.I. Lukomski, ''Composition Dependence of the Band Gap of $CuInS_{2x}Se_{2(1-x)}$'', Phys. Stat. Solidi (B) 105 (1981) K143.
11. S.J. Fonash, Solar Cell device Physics, Academic Press, New York, 1981.
12. H.L. Hwang, C.Y. Sun, C.Y. Leu, C.C. Cheng, C.C. Tu, ''Growth of $CuInS_2$ and its characterization'', Rev. Phys. Appl. 13 (1978) 745.
13. R. L. Anderson, ''Germanium- gallium arsenide heterojunctions'', IBM J.Res.Dev.4, 283, 1960.
14. B. MBOW, A. MEZERREG, N. REZZOUG, and C.LLINARES, ''Calculated and Measured Spectral Responses in Near-Infrared of III-V Photodetectors Based on Ga, In, and Sb'', phys. Stat. Sol. (a) 141, 511 (1994).
15. H. J. HOVEL and J. M. WOODALL,''$Ga_{1-x}Al_xAs$ - GaAs P-P-N Heterojunction Solar Cells'', J. Electrochem. Soc. 120, 1246 (1973).
16. H. J. HOVEL and J. M. WOODALL, 10th IEEE Photovoltaic Specialists Conf., Palo Alto (Calif.) 1973 (p.25).
17. A. LAUGIER and U. A. ROGER, Les photopiles solaires, Technique et Documentation, Paris 1981.

18. H. LUQUET, L. GOUSKOV, M. PEROTIN, A. JEAN, A. RJEB, T. ZAROURI, and G. BOUGNOT, ''Liquid- phase-epitaxial growth of $Ga_{0.96}Al_{0.04}Sb$: Electrical and photoelectrical characterizations'', J. appl. Phys. 60, 3582 (1986).
19. Michelle Schatzman, cours et exercices, analyse numerique,''Une approche mathematique'', 2001, 2e édition, DUNOD, p.211.
20. Henry Mathieu, cours, ''physique des semiconducteurs et des composants electroniques'', 2001, 5e édition, DUNOD, p. 124.
21. H. J. HOVEL, '' Semiconductors and Semimetals: Solar Cells'', 11, Academic Press, New York, 127 (1975).
22. Alain Ricaud, ''Photopiles Solaires'', de la physique de la conversion photovoltaïque aux filières, matériaux et procédés. 1997, 1e édition, Presses polytechniques et universitaires romandes, p.40.
23. E.M. Keita, B. Mbow, M.S. Mane, M.L. Sow, C. Sow, C. Sene ''Theoretical Study of Spectral Responses of Homojonctions Based on $CuInSe_2$'' Journal of Materials Science & Surface Engineering, Vol. 4 (4), 2016, pp392-399.